Journal of the American Chemical Society 137.28 (2015): 8991-8997

DOI: http://dx.doi.org/10.1021/jacs.5b02808

Energy Level Tuning of Non-fullerene Acceptors in Organic Solar Cells

Kjell Cnops,[1,2] German Zango,[3] Jan Genoe,[1,2] Paul Heremans,[1,2] M. Victoria Martinez-Diaz,[3] Tomas Torres[,3,4], David Cheyns,[*,2]*

[1] ESAT, KU Leuven, Kasteelpark Arenberg 10, B-3001 Leuven (Belgium)

[2] Imec, Kapeldreef 75, B-3001 Leuven (Belgium)

[3] Department of Organic Chemistry, Universidad Autónoma de Madrid, c/Francisco Tomás y Valiente 7, Cantoblanco, 28049 Madrid (Spain)

[4] IMDEA-Nanociencia, c/Faraday 9, Campus de Cantoblanco, 28049 Madrid (Spain)

ABSTRACT

The use of non-fullerene acceptors in organic photovoltaic devices could lead to enhanced efficiencies due to increased open-circuit voltages (V_{OC}) and improved absorption of solar light. Here we systematically investigate planar heterojunction devices comprising peripherally substituted subphthalocyanines as acceptor, and correlate device performance with heterojunction energetics. Due to a balance between V_{OC} and photocurrent, tuning of the interface energy gap is necessary to optimize power conversion efficiency in these devices. In addition, we explore the role of the charge transport layers in the device architecture. It is found that non-fullerene acceptors require adjusted buffer layers with aligned electron transport levels to enable efficient charge extraction, while the insertion of an exciton blocking layer at the anode interface further boosts photocurrent generation. These adjustments result in a planar heterojunction OPV device with 6.9% efficiency and a V_{OC} above 1 V.

INTRODUCTION

Solar energy conversion in organic photovoltaic (OPV) devices generally relies on the dissociation of photo-generated excitons at the heterojunction between an electron donating and an electron accepting material. The free energy driving this charge transfer process is related to the energetic offset between the excitonic state and the charge separated state. Transient absorption studies have shown that a reduction of this energetic driving force decreases the quantum yield of free charge carriers.[1,2] As a consequence, efficient photocurrent generation is only observed when sufficient band energy offsets are present at the heterojunction.[3,4] On the other hand, the open-circuit voltage (V_{OC}) of OPV devices has been shown to scale with the interface energy gap E_{DA}, being the energy difference between the highest occupied molecular orbital (HOMO) of the donor and the lowest unoccupied molecular orbital (LUMO) of the acceptor.[5,6] Photocurrent and V_{OC} are thus both governed by the heterojunction energetics. Energy level engineering of the active materials will therefore be crucial to further enhance the power conversion efficiency (PCE) of OPV devices.

The use of fullerenes as acceptor in OPV devices generally enables efficient charge transfer and electron transport. However, fullerene molecules possess a low absorption intensity at longer visible wavelengths and their frontier molecular orbital levels cannot easily be tuned. As a consequence, performance enhancement of OPV devices has mainly been achieved by development of new donor materials.[7,8] Chemical functionalization of small-molecule or polymer donor materials either adjusts the bandgap to enhance light absorption and photocurrent, or shifts the HOMO level to increase the charge transfer (CT) state energy and V_{OC}. However, the V_{OC} of efficient fullerene-based OPV devices is generally limited below 1 V due to the small optical bandgap of fullerene acceptors.[3] Therefore, it has been suggested that non-fullerene acceptors could enable an increased V_{OC} in OPV devices without sacrificing photocurrent generation.

Furthermore, non-fullerene acceptors offer additional advantages compared to fullerenes, such as efficient absorption of solar light and the easy band energy tuning by chemical modification.

Boron subphthalocyanine chloride (SubPc) is an organic semiconducting molecule commonly used as electron donor material in OPV devices.[9,10] In combination with fullerene acceptors, power conversion efficiencies above 5% have been reported.[11,12] However, SubPc can also be employed as acceptor material, provided that the selected donor material supplies sufficient energy offsets to enable efficient exciton dissociation at the heterojunction.[13,14] The electronic properties of SubPc molecules can be easily tuned by introduction of peripheral substituents.[9] Similar to halogenated phthalocyanines,[15] peripheral halogenation results in a shift of the molecular orbital energy levels, enabling the use of these SubPc derivatives as acceptors in combination with common donor materials.

In contrast, axial substitution of the chlorine atom has shown little effect on the molecular orbital levels.[10] Because neither peripheral nor axial substitutions alter the conjugated system of the molecule, the optical bandgap and absorption spectrum of SubPc derivatives remain largely unchanged. Consequently, the class of SubPc molecules is highly suited to investigate the influence of the acceptor's energetic position on OPV device performance. Moreover, the easy tunability of their energy levels simplifies the optimization of interface energetics in donor-acceptor heterojunctions. Both peripherally and axially substituted SubPc molecules have been applied as electron acceptor material in previous reports, resulting in high-voltage devices with V_{OC} up to 1.3 V.[16–18] However, low quantum efficiencies and the overlapping absorption profiles of donor and acceptor materials resulted in low photocurrent generation. Selecting donor materials with complementary absorption profiles to the SubPc acceptors has resulted in efficiencies over 6%.[19] Partially or fully peripherally halogenated SubPc-Cl (namely, F_{12}-SubPc-Cl and Cl_6-SubPc-

Cl) have been extensively incorporated in OPV devices in the last few years, thus suggesting the need of a fine-tuning of the HOMO and specially LUMO levels of the acceptor compound in the corresponding active layer. In this study we combine four small-bandgap donor materials with four SubPc derivatives as acceptor in vacuum-evaporated planar heterojunction OPV devices. Specifically, we have explored for the first time, an unsymmetrically substituted SubPc bearing two chlorine atoms at two isoindole units, Cl4-SubPc-Cl, as a compound with a slight increase of the LUMO energies compared to Cl_6-SubPc-Cl. Moreover, novel electron-accepting groups such as cyano, have been introduced as peripheral substituents, giving access to new evaporable electron–acceptor $(CN)_3$-SubPc-F bearing π-conjugated substituents and an intermediate electron-withdrawing character, between C_{l6}-SubPc-Cl and F_{12}-SubPc-Cl. By altering the peripheral substituent groups on the SubPc molecule the electron affinity of these non-fullerene acceptors is tuned in this particular case over 0.3 eV. However, the LUMO level of SubPcs can be lowered further introducing appropriate electron-withdrawing peripheral substituents. Thus, taking as reference the non-substituted SubPc-Cl one can formally increase the mentioned range until even 1eV.[9] This allows to systematically study the effect of heterojunction energetics on device performance, while the complementary absorption profiles of donor and acceptor materials results in high photocurrent generation. The highest PCE is obtained for the combination of boron subnaphthalocyanine chloride (SubNc) as donor and hexachlorinated SubPc (Cl_6-SubPc-Cl) as acceptor. The device performance is further improved by replacing the molybdenum oxide (MoO_3) hole transport layer (HTL) by a diindenoperylene exciton blocking layer, resulting in a planar heterojunction OPV device with 6.9% efficiency and a V_{OC} above 1 V.

RESULTS AND DISCUSSION

Four peripherally substituted SubPc derivatives, shown in **Figure 1a**, were used in this study: two partially chlorinated SubPc molecules (Cl_4-SubPc-Cl and Cl_6-SubPc-Cl), a fully fluorinated SubPc molecule (F_{12}-SubPc-Cl), and a tricyanated SubPc molecule ($(CN)_3$-SubPc-F);[20] where the latter contains a fluoride as axial ligand, instead of a chloride. All four SubPc derivatives have very similar absorption spectra in solution (**Figure S1**), peaking at wavelengths around 570 nm. The electron affinities of these molecules, indicative of their LUMO energies, were estimated from the reduction potential obtained by cyclic voltammetry measurements (**Figure S2**), and are schematically depicted in **Figure 1c**. The electron withdrawing character of the peripheral substituents lowers the frontier orbital energies of the SubPc molecule, resulting in LUMO energies ranging from -3.54 eV to -3.85 eV. We note that caution should be used when comparing these LUMO levels with molecular energy levels in literature.[21] First of all, cyclic voltammetry measurements yield an approximate value of the electron affinity (and LUMO energy). Secondly, literature employs many different approaches to measure and report molecular energy levels, and the experimental error is often large. Therefore, the indicated LUMO levels and interface bandgap energies in this work only serve to reflect the relative positions of the transport energy levels for the different SubPc derivatives, rather than representing the absolute values of these energy levels. Planar heterojunctions devices were fabricated comprising the SubPc derivatives as acceptor. These non-fullerene acceptors were combined with the small-bandgap donor materials shown in **Figure 1b**: lead phthalocyanine (PbPc), zinc phthalocyanine (ZnPc), SubNc, and tetra-fluoro zinc phthalocyanine (F_4-ZnPc). These donor molecules were selected to span a range of HOMO energy levels: -5.0 eV, -5.11 eV, -5.37 eV, and -5.46 eV, respectively.[22–24] Due to their smaller bandgap, all donor materials have absorption spectra complementary to the SubPc acceptors (**Figure S3**). A 14 nm thick donor layer was deposited for SubNc, while a thickness of 40 nm was chosen for the

other phthalocyanine donors. The thickness of the acceptor layer was set at 8 nm, irrespective of which SubPc derivative was used. Insertion of 5 nm MoO_3 at the anode interface ensures good hole extraction due to an improved energy level alignment with the donor materials.[25] A 50 nm thick 1:1 blend of bathocuproine (BCP) and fullerene C_{60} was used as electron transport layer (ETL). The low optical absorption and high conductivity of this layer ensures sufficient optical spacer thickness without compromising electron extraction.[26] It has been shown that the presence of fullerene in the ETL does not actively contribute to the photocurrent generation in devices with a SubPc derivative as acceptor.[19,27] The role of the SubPc acceptor on device performance was studied by current density-voltage (*J*-*V*) measurements under simulated solar illumination of 100 mW/cm^2 (**Figure S4**). The combination of each SubPc derivative with several donor materials results in a large set of data (**Table S1**), enabling us to assess the impact of the heterojunction energetics on V_{OC}, FF, and photocurrent.

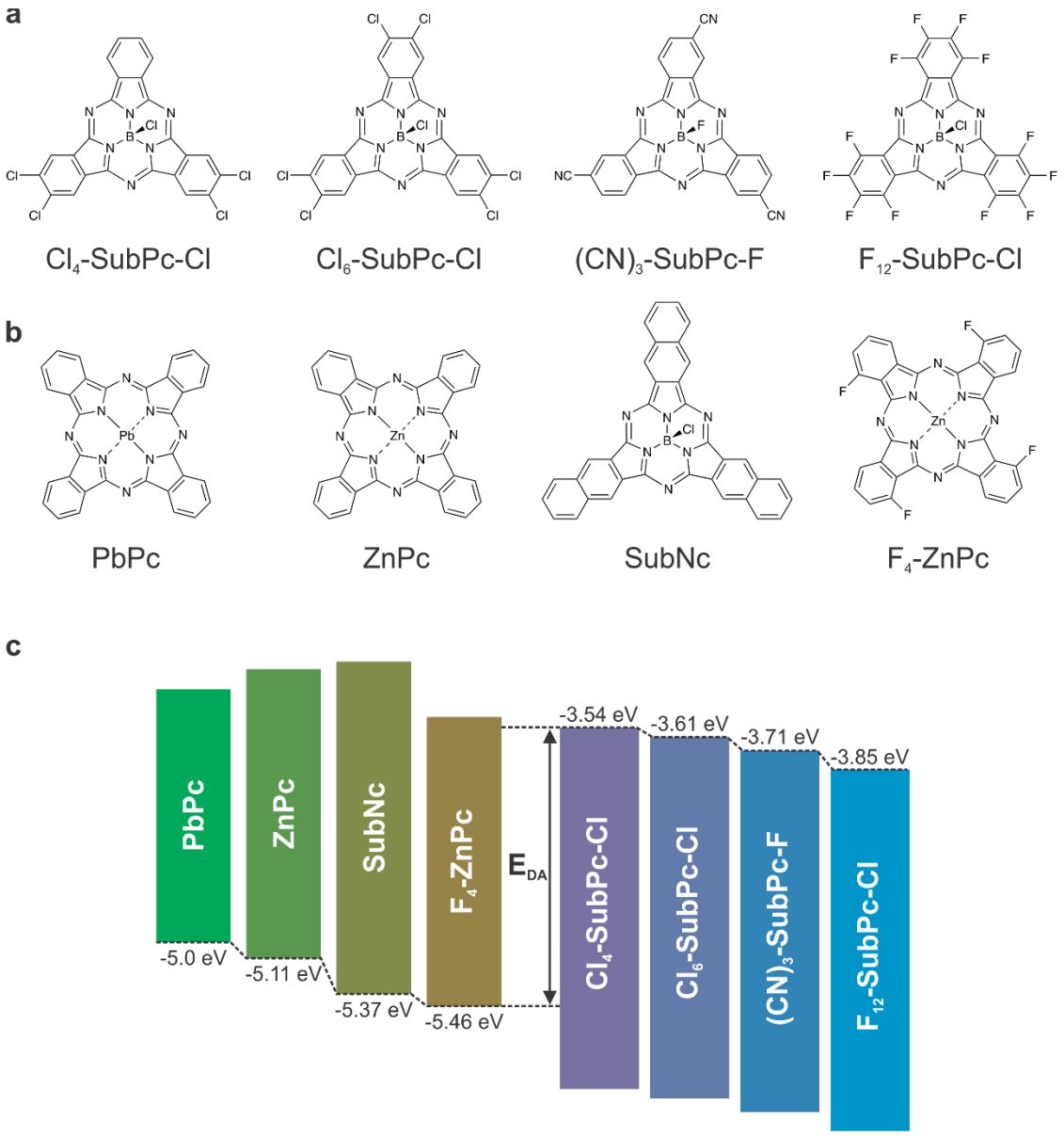

Figure 1: Structural and energetic properties of the active organic molecules used in this work. (a) Molecular structure of the SubPc acceptors. (b) Molecular structure of the donor materials. (c) Schematic representation of the LUMO energy levels of the SubPc acceptors, the HOMO energy levels of the donor materials, and the interface bandgap E_{DA}.

In this set of bilayer heterojunction devices the V_{OC} ranges from 0.3 V to 1.1 V. For a single donor material the V_{OC} can be tuned by 0.3 V depending on the choice of the SubPc acceptor. **Figure 2a**

shows that V_{OC} increases linearly with the interface energy gap E_{DA}. This corresponds to the well-known trend previously reported in literature,[5,6] correlating V_{OC} with the interface energetics. The upper limit for V_{OC} is determined by energy of the CT-state,[28] which is closely related to the interface gap E_{DA}. However, the measured V_{OC} in organic heterojunction devices never reaches this upper limit due to energy losses resulting from charge carrier recombination. The linear increase of V_{OC} with E_{DA} thus suggests that the different recombination processes occurring in these planar heterojunction devices generally don't influence V_{OC}. Only devices with a F_4-ZnPc donor yield a reduced V_{OC} compared to the other donor materials, possibly resulting from significantly increased recombination losses. However, the reduced V_{OC} could also be a related to dipole formation at the F_4-ZnPc interface, as was suggested after similar observations for fullerene-based devices.[29] Also considering the large uncertainty on the reported frontier orbital energies in literature, both interface energetics and recombination dynamics at non-fullerene heterojunctions are therefore subject to further investigation. The remarkably low V_{OC} for the device with the largest interface gap, i.e. the combination of F_4-ZnPc and Cl_4-SubPc-Cl, is a consequence of the lack of photocurrent generation at this heterojunction. With no free charge carriers available, no considerable photovoltage can be generated in this device structure.

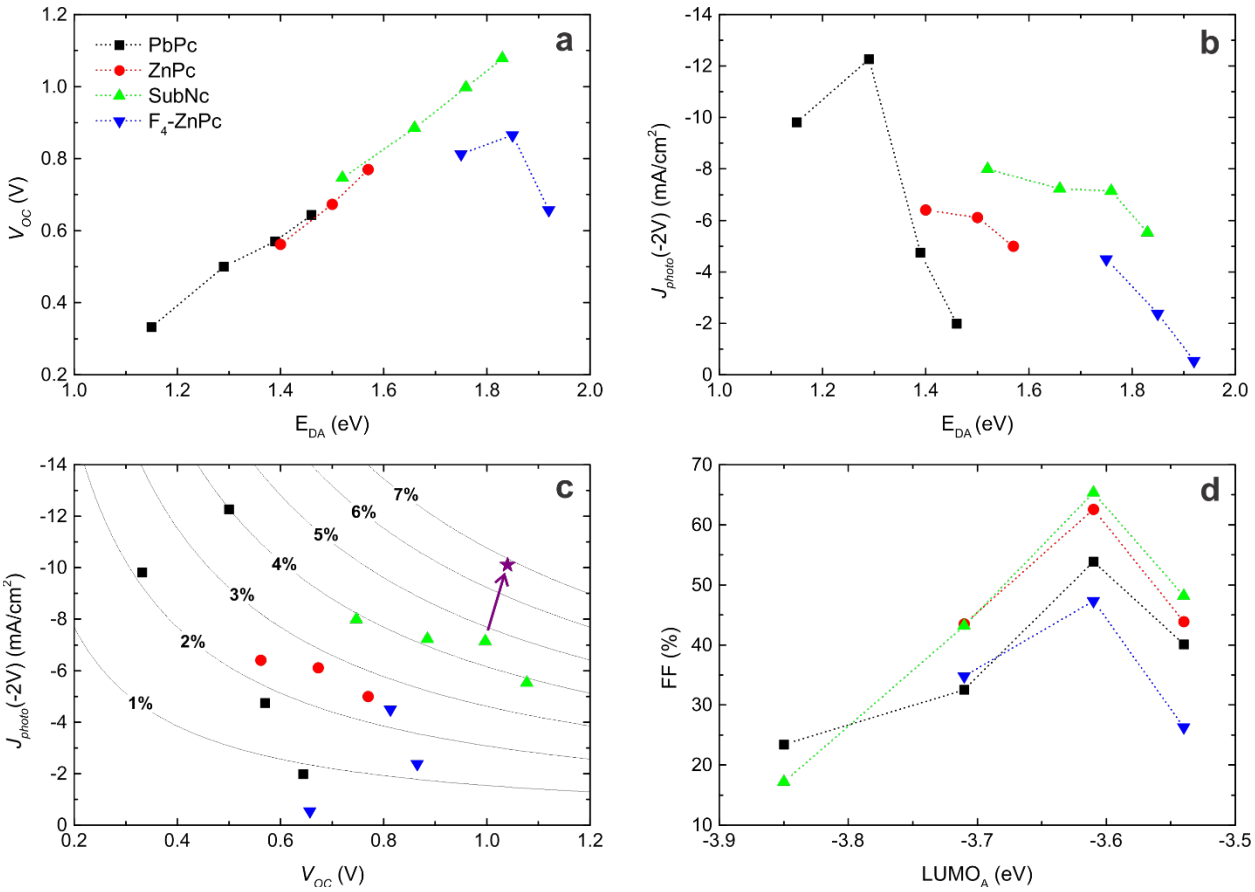

Figure 2: Relation of OPV performance parameters to the heterojunction energetics. (a) The V_{OC} scales linearly with the interface bandgap energy E_{DA}. (b) The photocurrent at reverse bias generally decreases with the interface bandgap energy E_{DA}. (c) The trade-off between photocurrent and V_{OC} limits the PCE of organic heterojunction devices. The contour lines represent the calculated PCE, assuming a 65% FF and a voltage-independent photocurrent. The arrow indicates a device with an exciton blocking hole transport layer, which increases the photocurrent and consequently PCE. (d) The FF is related to the LUMO energy of the acceptor.

The lack of photocurrent generation in the F_4-ZnPc/Cl_4-SubPc-Cl device warrants further investigation of the photocurrent dependence on the heterojunction energetics. Dissociation of bound excitons into free charge carriers is assumed to proceed through an intermediate CT-state.

A high quantum yield of free charge carriers is only obtained if this charge transfer process is energetically favorable. As the interface energy gap E_{DA} is closely related to the CT-state energy, a correlation of E_{DA} with photocurrent generation is expected. In **Figure 2b** we examine the photocurrent for all studied donor-acceptor heterojunctions in relation to their interface gap. Since the different SubPc derivatives all have similar absorption spectra, the photocurrent density in these devices is a good indication of their internal quantum efficiency. We evaluate the photocurrent density at reverse bias (-2 V), as the photocurrent at short-circuit conditions is reduced by charge extraction issues in some device structures (see below). Figure 2b reveals a general trend toward low photocurrent generation at large E_{DA} for all donor materials. Similar to previous reports,[1–4] the reduced photocurrent is a consequence of the smaller free energy driving the charge transfer process. The maximal interface gap where efficient charge transfer still occurs differs for every donor material, and depends on the optical bandgap of the donor. For example, devices with a SubNc donor, which has the largest bandgap of the studied donor materials, can generate reasonable photocurrent with all SubPc acceptors. In contrast, for devices containing PbPc, the smallest bandgap donor in our study, the photocurrent is significantly reduced when E_{DA} increases. In case of the F_4-ZnPc/Cl_4-SubPc-Cl heterojunction, E_{DA} is too large and the CT-state energy equals or exceeds the donor exciton energy. As a consequence, no free charges are generated at the heterojunction, and nearly no photocurrent is produced in this device structure.

Figure 2a and 2b make clear that V_{OC} and photocurrent exhibit opposite trends with respect to the interface energy gap E_{DA}: while V_{OC} linearly increases with E_{DA}, photocurrent generally decreases for large E_{DA}. As a result of this trade-off between V_{OC} and photocurrent, efficiency enhancement of a heterojunction OPV device relies on optimization of the interface energy gap. Both E_{DA} and V_{OC} should be maximized without substantial reduction of the photocurrent. **Figure 2c** illustrates

this trade-off for the presented planar heterojunction devices. With the contour lines indicating the calculated PCE, assuming a 65% FF and a voltage-independent photocurrent, we expect the highest PCE for the combination of a SubNc donor with a Cl_6-SubPc-Cl acceptor. Disregarding possible variations in FF, all remaining donor-acceptor pairs yield either a reduced V_{OC} or photocurrent, and consequently cannot obtain higher efficiencies. For a specific donor material, however, the PCE can easily be maximized by selecting the most appropriate acceptor material. The LUMO level tunability of the SubPc derivatives thus offers an additional advantage in PCE enhancement of heterojunction OPV devices.

Figure 2d plots the measured FF as a function of the LUMO energy of the SubPc acceptors. While the Cl_6-SubPc-Cl acceptor yields FFs up to 66%, severe S-kinks in the JV-curve reduce the FF below 25% for the F_{12}-SubPc-Cl acceptor. Such S-kinks occur in planar heterojunction devices when injection or extraction barriers are present at the interface between the active layers and the charge transport layers.[30] Because the FF is mainly determined by the choice of acceptor material in our device set, we conclude that the energy alignment at the acceptor/ETL interface is critical to avoid S-kink manifestation. As electron extraction in the BCP:C_{60} ETL likely occurs through percolating conductive pathways of fullerene molecules, this blend functions as an excellent ETL for fullerene acceptors.[26] However, a BCP:C_{60} ETL likely gives rise to charge injection or extraction barriers in combination with most non-fullerene acceptors, and energy level alignment between the SubPc acceptor and C_{60} is required to achieve high FFs. Clearly, Cl_6-SubPc-Cl fulfills this requirement, which explains the highly efficient devices obtained in previous work.[19] The remaining acceptor materials either form an extraction (F_{12}-SubPc-Cl and $(CN)_3$-SubPc-F) or injection barrier (Cl_4-SubPc-Cl) with the BCP:C_{60} ETL, resulting in reduced FFs. (While the C_{60} LUMO energy is often reported around 3.9 eV,[5] we repeat that the reported Cl_6-SubPc-Cl LUMO

energy of 3.61 eV is only approximate, and the claimed energy alignment is thus within experimental uncertainty.)

With an average FF of 65.3%, the SubNc/Cl_6-SubPc-Cl heterojunction indeed yields the highest PCE in this systematic study, as expected from Figure 2c. Due to a voltage-dependent photocurrent the average PCE is yet limited to 3.9% in the general device structure, comprising MoO_3 as HTL and BCP:C_{60} as ETL. Specific modification of these transport layers can however further enhance performance of these planar heterojunction devices. **Figure 3** shows the JV-curves for the following device structures with adjusted electron and hole transport layers, and **Table 1** summarizes the performance parameters of the best performing cells for each devices structure.

A: ITO/ MoO_3 (5 nm)/ SubNc (14 nm)/ F_{12}-SubPc-Cl (8 nm)/ BCP:C_{60} (1:1, 50 nm)/ Ag

B: ITO/ MoO_3 (5 nm)/ SubNc (14 nm)/ F_{12}-SubPc-Cl (8 nm)/ BCP:Yb (5%, 50 nm)/ Ag

C: ITO/ PEDOT:PSS/ DIP (5 nm)/ SubNc (14 nm)/ F_{12}-SubPc-Cl (8 nm)/ BCP:Yb (5%, 50 nm)/ Ag

D: ITO/ MoO_3 (5 nm)/ SubNc (14 nm)/ Cl_6-SubPc-Cl (8 nm)/ BCP:C_{60} (1:1, 50 nm)/ Ag

E: ITO/ PEDOT:PSS/ DIP (5 nm)/ SubNc (14 nm)/ Cl_6-SubPc-Cl (8 nm)/ BCP:C_{60} (1:1, 50 nm)/ A

In device structures with a F_{12}-SubPc-Cl acceptor layer, we replaced the BCP:C_{60} ETL with an Yb-doped BCP layer. The high conductivity of this BCP:Yb layer ensures a good electron extraction, even at the high thickness needed in our devices structures.[31] Figure 3 illustrates that the severe S-kink in device **A** is no longer present for the BCP:Yb ETL in device **B**, confirming that BCP:C_{60} indeed impedes electron extraction from the F_{12}-SubPc-Cl acceptor. We notice however that a parasitic photoshunt effect in these devices limits the FF to 57%. We observe that the photocurrent slope at reverse bias does not depend on the choice of the electron transport layer. The origin of the photoshunt is therefore likely related to bulk effects in the active layers of the

device.[32,33] In Cl_6-SubPc-Cl-based devices, for which S-kinks were not present, replacement of the ETL does not significantly affect the FF. However, the photocurrent is slightly reduced with BCP:Yb as ETL, which could result from exciton quenching by Yb-clusters in the ETL or slight changes in the optical interference pattern.

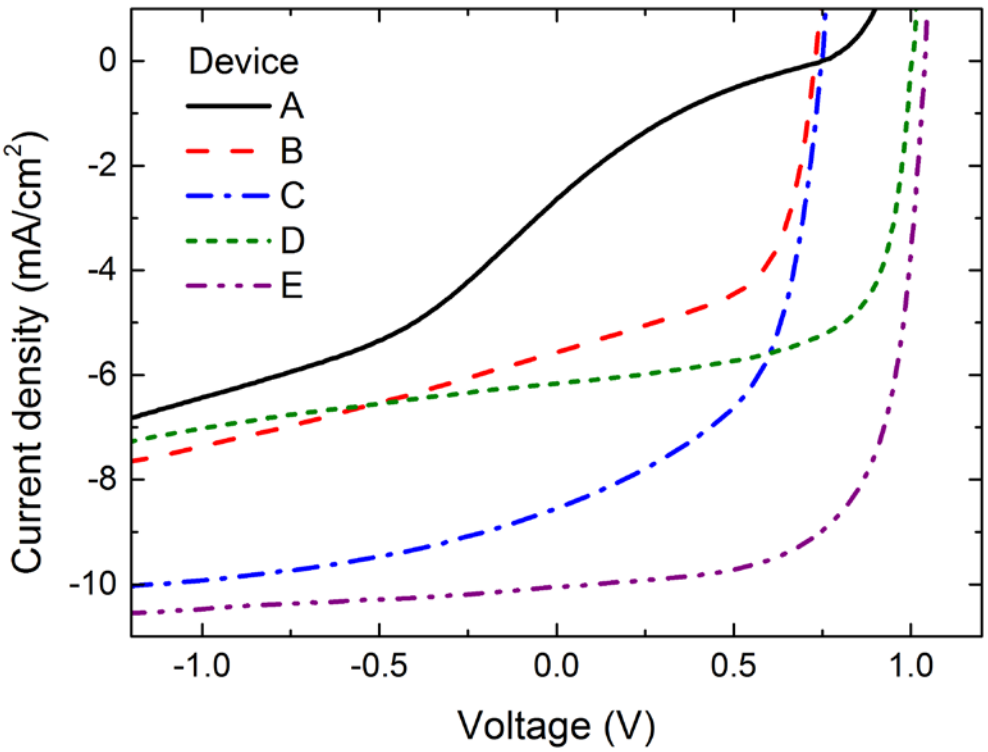

Figure 3: Current density-voltage measurements under simulated solar illumination for planar heterojunction devices with different electron and hole transport layers: (A) MoO_3 /SubNc / F_{12}-SubPc-Cl/ BCP:C_{60}, (B) MoO_3/ SubNc/ F_{12}-SubPc-Cl/ BCP:Yb, (C) PEDOT:PSS/ DIP/ SubNc/ F_{12}-SubPc-Cl/ BCP:Yb, (D) MoO_3/ SubNc/ Cl_6-SubPc-Cl/ BCP:C_{60}, and (E) PEDOT:PSS/ DIP/ SubNc/ Cl_6-SubPc-Cl/ BCP:C_{60}.

Table 1: Solar cell performance parameters for planar heterojunction devices with different electron and hole transport layers. For each device structure the open-circuit voltage (V_{OC}), short-circuit current density (J_{SC}), fill factor (FF), and power conversion efficiency (PCE) of the best performing cell are given.

Device structure	V_{OC} (V)	J_{SC} (mA/cm^2)	FF (%)	PCE (%)
A: MoO_3/ SubNc/ F_{12}-SubPc-Cl/ BCP:C_{60}	0.75	2.64	17.4	0.34
B: MoO_3/ SubNc/ F_{12}-SubPc-Cl/ BCP:Yb	0.73	5.57	57.6	2.25
C: PEDOT:PSS/ DIP/ SubNc/ F_{12}-SubPc-Cl/ BCP:Yb	0.75	8.55	53.4	3.31
D: MoO_3/ SubNc/ Cl_6-SubPc-Cl/ BCP:C_{60}	1.00	6.17	65.9	3.96
E: PEDOT:PSS/ DIP/ SubNc/ Cl_6-SubPc-Cl/ BCP:C_{60}	1.04	10.1	66.6	6.86

At the anode interface of the device structure, a MoO_3 HTL was used to ensure efficient hole extraction from the donor layers.[25] Unfortunately MoO_3 also significantly reduces the photocurrent due to quenching of donor excitons at its interface.[34,35] The introduction of exciton blocking[12,36] or exciton dissociating HTLs[24] has been shown to significantly improve photocurrent generation in planar heterojunction devices. Recently diindenoperylene (DIP) was introduced as exciton blocking HTL for SubNc-based devices.[19] Here, a spin-coated poly(3,4-ethylenedioxythiophene):poly(styrenesulfonate) (PEDOT:PSS) layer is needed to provide a smooth surface, ensuring that DIP forms a closed layer during evaporation. Indeed, the replacement of MoO_3 by DIP increases the short-circuit current density (J_{SC}) by 54% in device **C**. Also V_{OC} slightly increases upon insertion of the exciton blocking DIP layer. With both ETL and HTL replaced in the SubNc/F_{12}-SubPc-Cl heterojunction device, the PCE of 3.31% is nearly a 10-fold increase compared to the original device structure. Also for the champion heterojunction, comprising a SubNc donor and Cl_6-SubPc-Cl acceptor (device **D**), the photocurrent is further

boosted by introducing an exciton blocking DIP layer at the anode (device **E**). The increased J_{SC} of 10.1 mA/cm^2 leads to further efficiency enhancement for this heterojunction, as illustrated in Figure 2c. Moreover, with a V_{OC} above 1 V and a FF of 67%, the resulting PCE of 6.9% is among the highest reported efficiencies for bilayer OPV devices with a non-fullerene acceptor.

CONCLUSION

In conclusion, we demonstrated the efficient use of SubPc derivatives as non-fullerene acceptors in bilayer heterojunctions devices. In a systematic study, we explored how the device performance depends on the LUMO energy level of these acceptors. Due to a trade-off between V_{OC} and photocurrent, the maximal PCE is obtained for heterojunctions with an optimized interface energy gap. Peripheral substitution of the SubPc acceptors enables this interface gap optimization, while the selection of the electron and hole transport layers is crucial to achieve high photocurrent generation and extraction. This study thus shows that the use of non-fullerene acceptors is a successful method to enhance the performance of organic solar cells. Further performance enhancement could results from advanced device structures, such as the insertion of a bulk heterojunction layer, or the extension to cascade architectures.

EXPERIMENTAL SECTION

The F_{12}-SubPc-Cl and Cl_6-SubPc-Cl compounds were synthesized as described in literature.[19,37] Cl_4-SubPc-Cl was prepared by cross condensation of 4,5-dichlorophthalonitrile[38] and phthalonitrile following the standard procedure. $(CN)_3$-SubPc-F was prepared by palladium-mediated cyanation of triiodo-SubPc-OPh^{t}Bu,[39] and subsequent phenoxy group to fluorine axial

exchange.[40] Further details about the synthesis of these SubPc derivatives are given in the Supporting Information.

Electrochemical measurements were performed with an Autolab PGStat 30 system using a three electrode configuration system. The measurements were carried out using THF solutions containing 0.1 M tetrabutylammonium hexafluorophosphate ($TBAPF_6$). A glassy carbon electrode (3 mm diameter) was used as the working electrode, and a platinum wire and an $Ag/AgNO_3$ (in CH_3CN) electrode were employed as the counter and the reference electrodes, respectively. Ferrocene (Fc) was added as an internal reference and all the potentials were given relative to the Fc/Fc^+ couple. The scan rate was 100 mV/s.

OPV devices were fabricated on pre-patterned indium tin oxide-coated glass substrates. Detergent and solvent cleaning of all substrates was followed by a 5-minute oxygen-plasma treatment to remove remaining carbon residue. PEDOT:PSS was spin-coated at 5000 rpm and followed by a bake-out at 130˚C in N_2. All organic materials were purified by thermal gradient sublimation before loading in a high-vacuum evaporation chamber. All materials were deposited at an evaporation rate of 1 Å/s. The 120 nm thick Ag cathode was evaporated through a shadow mask defining an active area of 13.4 mm^2.

Current density-voltage characteristics were measured under simulated solar illumination, using a Keithley 2602 measurement unit and an Abet solar simulator, calibrated with a Fraunhofer certified photovoltaic cell to yield a 100 mW/cm^2 AM1.5G spectrum.

ASSOCIATED CONTENT

Supporting Information Synthetic procedures, absorption spectra, cyclic voltammograms, extinction coefficients, and current density-voltage measurements under simulated solar illumination. This material is available free of charge via the Internet at http://pubs.acs.org.

AUTHOR INFORMATION

Corresponding authors

tomas.torres@uam.es

david.cheyns@imec.be

ACKNOWLEDGEMENTS

The research leading to these results has received funding from the European Community's Seventh Framework Programme (FP7/2007-2013) under grant agreement 287818 of the X10D project and from the European Community's ERC Advanced Grant # 320680 (EPOS CRYSTALLI). This work is also supported by the Spanish MINECO (CTQ-2014-52869-P) and Comunidad de Madrid (S2013/MIT-2841, FOTOCARBON). The authors want to thank Erwin Vandenplas for processing support.

REFERENCES

(1) Ohkita, H.; Cook, S.; Astuti, Y.; Duffy, W.; Tierney, S.; Zhang, W.; Heeney, M.; Mcculloch, I.; Nelson, J.; Bradley, D. D. C.; Durrant, J. R. *J. Am. Chem. Soc.* **2008**, *130*, 3030.

(2) Shoaee, S.; Clarke, T. M.; Huang, C.; Barlow, S.; Marder, S. R.; Heeney, M.; Mcculloch, I.; Durrant, J. R. *J. Am. Chem. Soc.* **2010**, *132*, 12919.

(3) Hoke, E. T.; Vandewal, K.; Bartelt, J. A.; Mateker, W. R.; Douglas, J. D.; Noriega, R.; Graham, K. R.; Fréchet, J. M. J.; Salleo, A.; McGehee, M. D. *Adv. Energy Mater.* **2012**, *3*, 220.

(4) Vandewal, K.; Ma, Z.; Bergqvist, J.; Tang, Z.; Wang, E.; Henriksson, P.; Tvingstedt, K.; Andersson, M. R.; Zhang, F.; Inganäs, O. *Adv. Funct. Mater.* **2012**, *22*, 3480.

(5) Wilke, A.; Endres, J.; Hörmann, U.; Niederhausen, J.; Schlesinger, R.; Frisch, J.; Amsalem, P.; Wagner, J.; Gruber, M.; Opitz, A.; Vollmer, A.; Brütting, W.; Kahn, A.; Koch, N. *Appl. Phys. Lett.* **2012**, *101*, 233301.

(6) Graham, K. R.; Erwin, P.; Nordlund, D.; Vandewal, K.; Li, R.; Ngongang Ndjawa, G. O.; Hoke, E. T.; Salleo, A.; Thompson, M. E.; McGehee, M. D.; Amassian, A. *Adv. Mater.* **2013**, *25*, 6076.

(7) Lin, Y.; Li, Y.; Zhan, X. *Chem. Soc. Rev.* **2012**, *41*, 4245.

(8) Mishra, A.; Bäuerle, P. *Angew. Chem. Int. Ed. Engl.* **2012**, *51*, 2020.

(9) Claessens, C. G.; González-Rodríguez, D.; Rodríguez-Morgade, M. S.; Medina, A.; Torres, T. *Chem. Rev.* **2014**, *114*, 2192.

(10) Morse, G. E.; Bender, T. P. *ACS Appl. Mater. Interfaces* **2012**, *4*, 5055.

(11) Pandey, R.; Zou, Y.; Holmes, R. J. *Appl. Phys. Lett.* **2012**, *101*, 033308.

(12) Lin, C.-F.; Nichols, V. M.; Cheng, Y.-C.; Bardeen, C. J.; Wei, M.-K.; Liu, S.-W.; Lee, C.-C.; Su, W.-C.; Chiu, T.-L.; Han, H.-C.; Chen, L.-C.; Chen, C.-T.; Lee, J.-H. *Sol. Energy Mater. Sol. Cells* **2014**, *122*, 264.

(13) Beaumont, N.; Cho, S. W.; Sullivan, P.; Newby, D.; Smith, K. E.; Jones, T. S. *Adv. Funct. Mater.* **2012**, *22*, 561.

(14) Cnops, K.; Rand, B. P.; Cheyns, D.; Verreet, B.; Empl, M. A.; Heremans, P. *Nat. Commun.* **2014**, *5*, 3406.

(15) Brinkmann, H.; Kelting, C.; Makarov, S.; Tsaryova, O.; Schnurpfeil, G.; Wöhrle, D.; Schlettwein, D. *Phys. Status Solidi* **2008**, *205*, 409.

(16) Gommans, H.; Aernouts, T.; Verreet, B.; Heremans, P.; Medina, A.; Claessens, C. G.; Torres, T. *Adv. Funct. Mater.* **2009**, *19*, 3435.

(17) Sullivan, P.; Duraud, A.; Hancox, I.; Beaumont, N.; Mirri, G.; Tucker, J. H. R.; Hatton, R. A.; Shipman, M.; Jones, T. S. *Adv. Energy Mater.* **2011**, *1*, 352.

(18) Morse, G. E.; Gantz, J. L.; Steirer, K. X.; Armstrong, N. R.; Bender, T. P. *ACS Appl. Mater. Interfaces* **2014**, *6*, 1515.

(19) Verreet, B.; Cnops, K.; Cheyns, D.; Heremans, P.; Stesmans, A.; Zango, G.; Claessens, C. G.; Torres, T.; Rand, B. P. *Adv. Energy Mater.* **2014**, *4*, 1301413.

(20) This compound is in fact a 1:3 mixture of C_3 and C_1 regioisomers.

(21) Bredas, J.-L. *Mater. Horiz.* **2014**, *1*, 17.

(22) Ikushima, A. J.; Kanno, T.; Yoshida, S.; Maeda, A. *Thin Solid Films* **1996**, *273*, 35.

(23) Riede, M. K.; Uhrich, C.; Widmer, J.; Timmreck, R.; Wynands, D.; Schwartz, G.; Gnehr, W.-M.; Hildebrandt, D.; Weiß, A.; Hwang, J.; Sundarraj, S.; Erk, P.; Pfeiffer, M.; Leo, K. *Adv. Funct. Mater.* **2011**, *21*, 3019.

(24) Barito, A.; Sykes, M. E.; Huang, B.; Bilby, D.; Frieberg, B.; Kim, J.; Green, P. F.; Shtein, M. *Adv. Energy Mater.* **2014**, *4*, 1400216.

(25) Hancox, I.; Sullivan, P.; Chauhan, K. V.; Beaumont, N.; Rochford, L. A.; Hatton, R. A.; Jones, T. S. *Org. Electron.* **2010**, *11*, 2019.

(26) Bartynski, A. N.; Trinh, C.; Panda, A.; Bergemann, K. J.; Lassiter, B. E.; Zimmerman, J. D.; Forrest, S. R.; Thompson, M. E. *Nano Lett.* **2013**, *13*, 3315.

(27) Verreet, B.; Rand, B. P.; Cheyns, D.; Hadipour, A.; Aernouts, T.; Heremans, P.; Medina, A.; Claessens, C. G.; Torres, T. *Adv. Energy Mater.* **2011**, *1*, 565.

(28) Vandewal, K.; Tvingstedt, K.; Gadisa, A.; Inganäs, O.; Manca, J. V. *Phys. Rev. B* **2010**, *81*, 125204.

(29) Meiss, J.; Merten, A.; Hein, M.; Schuenemann, C.; Schäfer, S.; Tietze, M.; Uhrich, C.; Pfeiffer, M.; Leo, K.; Riede, M. *Adv. Funct. Mater.* **2012**, *22*, 405.

(30) Tress, W.; Leo, K.; Riede, M. K. *Adv. Funct. Mater.* **2011**, *21*, 2140.

(31) Mityashin, A.; Cheyns, D.; Rand, B. P.; Heremans, P. *Appl. Phys. Lett.* **2012**, *100*, 053305.

(32) Renshaw, C. K.; Zimmerman, J. D.; Lassiter, B. E.; Forrest, S. R. *Phys. Rev. B* **2012**, *86*, 085324.

(33) Jeong, W.-I.; Lee, Y. E.; Shim, H.-S.; Kim, T.-M.; Kim, S.-Y.; Kim, J.-J. *Adv. Funct. Mater.* **2012**, *22*, 3089.

(34) Xiao, X.; Zimmerman, J. D.; Lassiter, B. E.; Bergemann, K. J.; Forrest, S. R. *Appl. Phys. Lett.* **2013**, *102*, 073302.

(35) Barito, A.; Sykes, M. E.; Bilby, D.; Amonoo, J.; Jin, Y.; Morris, S. E.; Green, P. F.; Kim, J.; Shtein, M. *J. Appl. Phys.* **2013**, *113*, 203110.

(36) Hirade, M.; Adachi, C. *Appl. Phys. Lett.* **2011**, *99*, 153302.

(37) Claessens, C. G.; González-Rodríguez, D.; del Rey, B.; Torres, T.; Mark, G.; Schuchmann, H.-P.; von Sonntag, C.; MacDonald, J. G.; Nohr, R. S. *Eur. J. Org. Chem.* **2003**, 2547.

(38) Wöhrle, D.; Eskes, M.; Shigehara, K.; Yamada, A. *Synthesis* **1993**, *2*, 194.

(39) Claessens, C. G.; Torres, T. *Tetrahedron Lett.* **2000**, *41*, 6361.

(40) Rodríguez-Morgade, M. S.; Claessens, C. G.; Medina, A.; González-Rodríguez, D.; Gutiérrez-Puebla, E.; Monge, A.; Alkorta, I.; Elguero, J.; Torres, T. *Chem. - Eur. J.* **2008**, *14*, 1342.

TABLE OF CONTENTS GRAPHIC

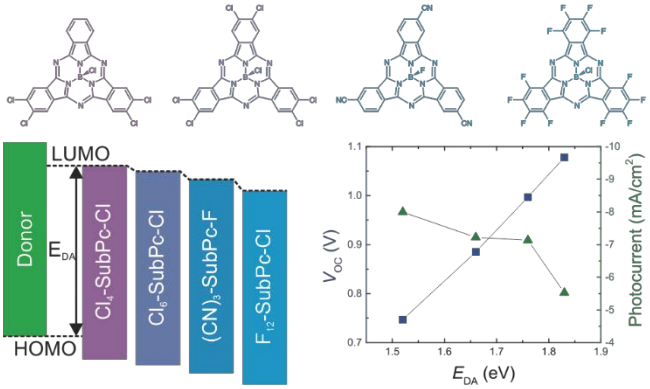

For Table of Contents Only